ISSN 0031-918X, Physics of Metals and Metallography, 2023, Vol. 124, No. 13, pp. 1579–1587. © Pleiades Publishing, Ltd., 2023.
ISSN 0031-918X, Physics of Metals and Metallography, 2023. © Pleiades Publishing, Ltd., 2023.

STRENGTH AND PLASTICITY

Microstructural Evolution and Mechanical Behavior of SP-700Ti Alloy during Superplastic Deformation

M. Morakabati[a], * and Amir Hossein Sheikhali[a]

[a] *Faculty of Materials and Manufacturing Technologies, Malek Ashtar University of Technology, Tehran, 193574521 Iran*

**e-mail: m_morakabati@mut.ac.ir*

Received December 28, 2022; revised June 12, 2023; accepted June 18, 2023

Abstract—In this paper, the superplastic behavior of SP-700 alloy (Ti–4.5Al–3V–2Mo–2Fe) was investigated by hot compression tests and hot tensile tests in the temperature range of 700–950°C and strain rates of 0.001 to 1 s^{-1}. The microstructural analysis and mechanical behavior of the alloy were studied during superplastic deformation. Although the elongation became higher than 370% at 700°C, the alloy showed a relatively high work hardening. At 750 and 800°C, the typical superplasticity was occurred and the specimens endured a large elongation of 427–440%. Microstructure of the alloy in 700–800°C was mainly consisted of globular α phase, while the globular α phase was completely removed in the tip fracture of the specimen deformed at 850°C due to deformation-induced transformation. In the temperature range of 850–950°C, the elongation was decreased to 250–325% as a consequence of the removal of α phase, significant β grain growth, and crack formation along β/β grain boundaries. The maximum elongation of 440% was obtained at 800°C where the strain-rate sensitivity is equal to 0.38 which is accommodated by the m-value distribution map of the alloy. During superplastic deformation in the single β phase region, the Rachinger grain boundary sliding (GBS) mechanism is the dominant phenomenon. However, deformation in the dual-phase α/β region is encouraged by dynamic recrystallization (DRX) and decomposition of α colonies.

Keywords: SP-700 alloy, Superplastic deformation, Hot tensile test, m-value distribution map, Deformation induced transformation

DOI: 10.1134/S0031918X2260213X

1. INTRODUCTION

SP-700 alloy is a dual-phase Ti base alloy with a chemical composition of Ti–4.5Al–3V2Mo–2Fe which was introduced in 1989 by the Nippon Kokan NKK company [1]. The SP-700 (β-rich alloy) has higher mechanical properties and lower superplastic temperature in comparison with the Ti–6Al–4V (α-rich alloy) [2, 3]. The Ti–6Al–4V alloy has superplastic behavior at temperatures higher than 900°C, while the α case formation decreased during the superplastic deformation of the SP-700 alloy due to its lower superplastic temperature [4].The superplasticity of dual-phase Ti alloys is extremely affected by β-phase content [5]. It is shown that the β phase is considerably softer than the α phase, especially at elevated temperatures which is attributed to high diffusion and more active slip systems in the β phase [6]. Thus, in either diffusion-accommodated, dislocation-accommodated superplasticity, or a combination of them, it can be considered that the content of the β phase has an important effect on determining the predominant accommodation mechanism [7]. The superplastic behavior of the SP-700 alloy was studied previously by researchers. For instance, Fukai et al. [4] investigated the superplastic properties of the SP-700 alloy such as *m*-value and flow stress without any microstructural investigations. They observed that the SP-700 alloy exhibits excellent m-value at a wide range of strain rates ($m > 0.5$) compared to the Ti–6Al–4V alloy. Shen et al. [7] studied the effect of the competitive dynamic recrystallization between α and β phases on the superplastic behavior of the SP-700 alloy. The results show that the superplasticity of the alloy can be explained by grain boundary sliding (GBS). It has been demonstrated that the rearranged dislocations are converted into high-angle sub-boundaries in α grains by continuous dynamic recrystallization (CDRX). However, the recrystallized β grains are dominantly induced by discontinuous dynamic recrystallization (DDRX), aided by CDRX. Alabort et al. [8] explained the deformation mechanisms responsible for the superplastic behavior in the Ti–6Al–4V and Ti–4Al–2.5V–1.5Fe alloys using the m-value characteristic. They found that the fine-grained microstructure is responsible for the superplasticity, $m > 0.3$, at low temperatures. Titanium alloys undergo work hardening, dynamic recovery (DRV), dynamic recrystallization [9, 10], dynamic globularization [11], and deformation-induced transformation (DIT) [12] during hot deformation, which are metallurgical phe-

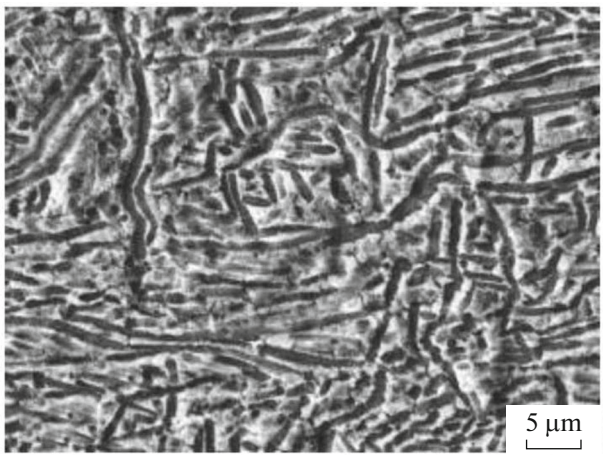

Fig. 1. The SEM image of the microstructure of the hot rolled alloy.

nomena controlling the microstructure and properties. It has been reported that phase transformation [13] and DRX [14], determined the superplasticity. Alabort et al. [5] demonstrated that when the subgrain size is greater than the average grain size, GBS is the dominant deformation mechanism of superplasticity, and the accommodation process is dislocation glide. The α to β transformation kinetics are accelerated during concurrent phase transformation and hot deformation, due to the strain-induced α/β phase transformation [15, 16]. Although studies were performed on the superplastic behavior of the SP-700 alloy in the last decades [1, 4, 7, 17–20], there is a leakage for study on superplastic forming of the SP-700 alloy from viewpoint of correlation between hot tensile test, hot compression test and microstructural analysis. The authors [15, 21, 22] studied the hot compression and hot torsion of the SP-700 alloy, previously. In this research, the superplastic behavior of the alloy was studied using the hot compression and the hot tensile tests in the temperature range of 700–950°C. The m-value distribution map has been generated as strain rate and temperature function. Then, the mechanical properties and microstructural evolution of the deformed specimens were examined and correlated.

2. EXPERIMENTAL

The SP-700 alloy was cast using a double vacuum arc remelting furnace. The homogenization of the ingot was carried out at 1150°C for 5 h. The chemical composition of the alloy was obtained as 4.4 Al, 2.85 V, 2.15 Mo, 2.1 Fe in weight percent, and the balance Ti using a TESCAN-VEGA3 scanning electron microscope equipped with Energy Dispersive Spectroscopy. The chemical composition of the ingot is within the acceptable range of the alloy according to AMS 4964 standard [23]. The metallographic method was used experimentally to determine the β transus temperature (T_β) [24]. The β transus temperature of the alloy determined as 930 ± 10°C. The authors [15, 21, 22] previously studied the hot working behavior of the SP-700 alloy by the hot compression and the hot torsion tests. They developed an ingot breakdown process at 850°C in the α/β phase region. Therefore, in this work, the ingot breakdown of it was performed at 850°C. The microstructure of the α/β hot-rolled plate of the alloy with a lamellar starting structure is shown in Fig. 1. The microstructure contains a 66% plate-like α phase with a thickness of 1–3 μm in the β matrix. Uniaxial compression tests were performed by an Instron 8502 machine equipped with a resistance furnace at 700, 800, 850, 900, and 950°C. The cylindrical hot compression test specimens were prepared following ASTM E209 [25]. A thin layer of graphite was rubbed on the contacting surface of the specimen and the anvils to minimize the friction. After holding at the test temperature for 10 min, the specimens were deformed at strain rates of 0.001, 0.1, and 1 s^{-1} to 50% reduction. To investigate the superplastic behavior of the α/β hot-rolled plate, the superplastic specimens were provided with a thickness of 3 mm, a gauge length of 10 mm, a gauge width of 6 mm, and a total length of 100 mm. The hot tensile tests were performed at 700, 750, 800, 850, 900, and 950°C with a constant strain rate of 0.005 s^{-1}. The water quenched specimens were sectioned parallel to the tension axis and prepared by the standard metallographic techniques according to ASTM E3 [26]. Then, the specimens were prepared by polishing and etched with a Kroll's reagent solution (92% H_2O + 5% HNO_3 + 3% HF) for a few seconds. The microstructural observations were conducted using an OLYMPUS light microscope and TESCAN-VEGA3 scanning electron microscope. The volume fraction and grain size of the phases were measured using Image J 1.44 analysis software. It should be mentioned that the dimensions of the phases reported is the average dimensions of them.

3. RESULTS AND DISCUSSION

3.1. The m-Value Distribution Map

The authors investigated the hot working behavior of the SP-700 alloy previously [15]. The hot deformation activation energy of the SP-700 alloy in the α/β region was determined as 305.5 kJ mol^{-1}, which is higher than that in the single-phase β region (165.2 kJ mol^{-1}) due to the dynamic globularization of the lamellar α phase. The peak efficiency of 54% was also observed in the processing map of the alloy the by authors [15] in the temperature range of 780–810°C and strain rates of 0.001–0.008 s^{-1}. The strain-rate sensitivity coefficient (m) can be calculated from the slope of $\ln\sigma$–$\ln\dot{\varepsilon}$ curves [27, 28]. The m-value distribution map of the hot compressed alloy as a function of strain rate and temperature is given in Fig. 2. It is

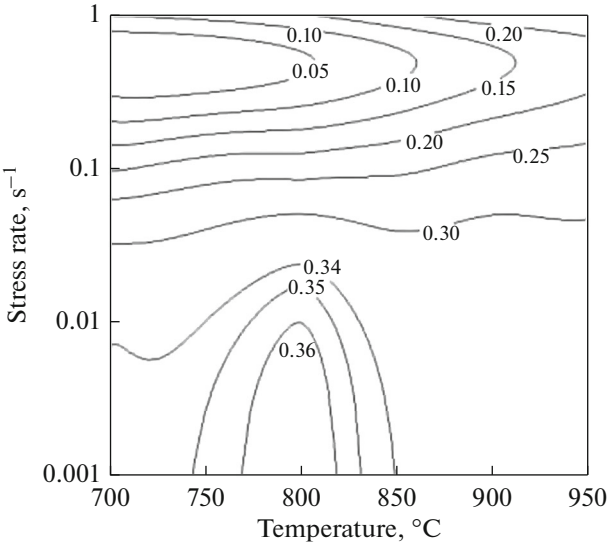

Fig. 2. The m-value distribution map of the hot compressed specimens as a function of strain rate and temperature (contours represent the m-value).

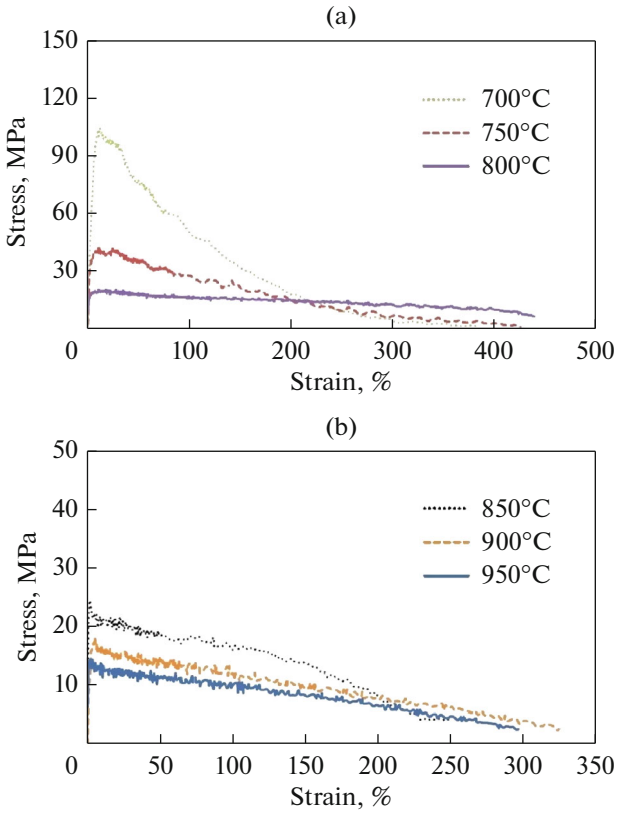

Fig. 3. The stress-strain curves of the alloy at a strain rate of 0.005 s^{-1} and temperatures of (a) 700, 750, 800; (b) 850, 900, 950°C.

seen that the m-values arise by decreasing the strain rate. However, the trend of the m-value has a complicated distribution as a function of temperature. The m-value increased by the temperature at strain rates of 0.1–1 s^{-1}, while it became higher than 0.34 at strain rates of 0.001–0.01 s^{-1} and a lower temperature range of 700–850°C. At strain rates of 0.001–0.01 s^{-1} and the temperature range of 770–820°C, the m-value became maximum, i.e., 0.36.

The α and β phases in titanium alloys have different lattice structures and mechanical properties. Since the β phase with BCC crystal structure has more active slip systems than the α phase with HCP crystal structure, the α phase has poor formability compared to the β phase. Therefore, the β matrix undergoes more significant deformation than the α phase, creating a greater possibility of dynamic recrystallization. Dynamic recrystallization at β grain boundaries corresponds to a high m-value [29]. On the other side, researchers [30–32] showed that the maximum m-value at low strain rates can be related to the optimum condition of the superplastic behavior. Regarding to Fig. 2, the superplastic behavior in the SP-700 alloy was more expected in the temperature range of 700–850°C and strain rates of 0.001–0.01 s^{-1}. Therefore, the superplastic hot tensile tests were performed in the temperature range of 700–950°C and a strain rate of 0.005 s^{-1}.

3.2. The Superplastic Behavior

The engineering stress-strain curves obtained from superplastic tensile tests at temperatures of 700, 750, 800, 850, 900, and 950°C and strain rate of 0.005 s^{-1} are depicted in Fig. 3. At temperature of 700°C, typical peak stress at a low strain of 6–12% followed by apparent flow softening. The flow softening generally implies the initiation of DRX, while it will be found from Section 3.3 that the flow softening is due to fragmentation of the lamellar α phase. On the other side, the flow curves comprise the yield point phenomenon (YPP). Wanjara [33] and Philippart [34] related the sudden decrease in flow stress after the yield stress to the solute drag effect. Therefore, for releasing dislocations and their subsequent motion, a high-stress level is required resulting in the appearance of peak stress. It has been also suggested [34] that the discontinuous yield in β Ti alloys is created by the high diffusion coefficient of interstitial atoms such as C, N, and O in the β phase and the formation of a Cottrel atmosphere around dislocations. The occurrence of discontinuous yield stress in the alloy can be caused by the high solution content of interstitial atoms, especially oxygen, which was determined as 1500 ppm. Regarding to Figs. 3 and 4, during deformation at 700°C, the alloy exhibits relatively high work hardening and tensile elongation of 372%. By increasing temperature to 750°C, the flow curve shows a weak work hardening, lower tensile stress, and the steady-state region. At 800°C, the maximum flow stress is 20 MPa. The m-

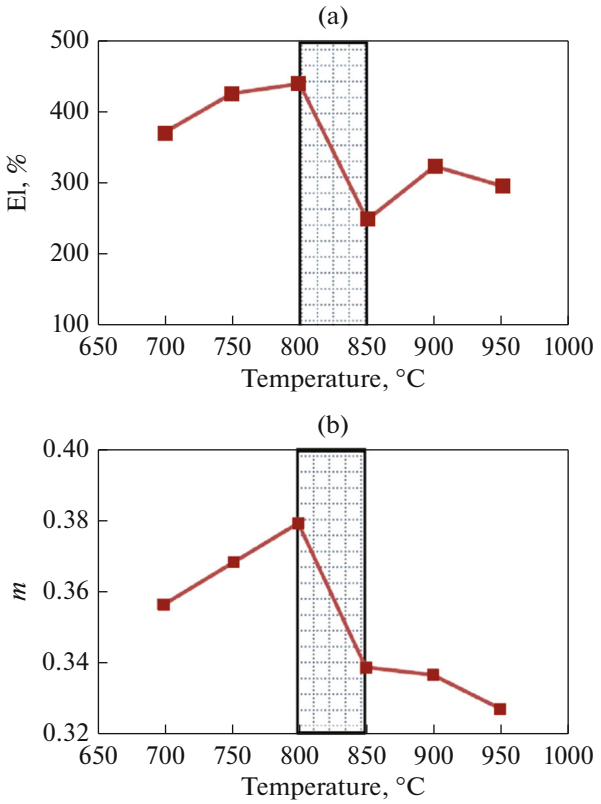

Fig. 4. Variation of (a) elongation, and (b) m-value of the alloy with temperature at strain rate of 0.005 s^{-1}.

value represents that the necking resistance is a significant parameter in superplastic deformation. The higher m-value reveals the better superplasticity of the materials [35]. Therefore, the typical superplastic deformation can occur at 800°C, and the specimen undergoes a significant elongation of 440% where the m-value becomes equal to 0.38. As the test temperature increases to 950°C, the peak stress reduces significantly due to easier dislocation movement. It is noteworthy that, at this temperature, the strain-rate sensitivity decreases to $m = 0.33$. It has been reported that [36, 37] the volume fraction and morphology of α and β phases play an essential role in the superplastic behavior of α/β Ti alloys. At temperatures higher than 850°C, the equilibrium of α and β phases changed by removing the α phase, resulting in a decrease in the elongation of the alloy. Hence, the specimens deformed in the temperature range of 850–950°C undergo a relatively lower elongation in 250 to 325% due to microstructural evolutions such as the disappearance of the α phase, grain growth, and crack formation along β/β grain boundaries. As will be mentioned in Section 3.3, as the disappearance of the α phase can be related to α → β deformation-induced transformation (DIT). As seen in Fig. 4, the m-values vary from 0.33 to 0.38, and a maximum elongation of 440% was obtained at 800°C, where the strain-rate sensitivity is maximum (0.38). Wisbey et al. [19] reported that the m-values of SP-700 alloy are between 0.4–0.5 in the temperature range of 700–800°C and strain rates of 10^{-5}–10^{-3} s^{-1}. They also indicated that the m-values of the alloy are between 0.3–0.4 at 850°C and at the same strain rates. As it is known [36], the higher m value leads to more significant elongation and a lower tendency of necking [36]. Therefore, it can be concluded that the optimum temperature for superplastic deformation of the alloy is in the temperature range of 750–800°C. Hence, the m value distribution map of the SP-700 alloy given in Fig. 2 could predict the optimal condition for superplastic deformation of the alloy very well.

3.3. Microstructure Characterization

The microstructure of the tip fracture region of the specimens deformed at temperatures of 700, 750, and 800°C and strain rate of 0.005 s^{-1} are shown in Fig. 5. As seen in Fig. 5a, the microstructure of the specimen deformed at 700°C consisted of lamellar α phase and globular α phase with a dimension of 2.3 μm. Whereas, only the globular α phase with a dimension of 6.8 μm can be observed in the microstructure of the specimen deformed at 750°C (Fig. 5b). Besides, by increasing the temperature from 700 to 800°C, the volume fraction of α phase decreased from 69.2 to 61.5%. The existence of equiaxed grains in the the specimen deformed at 800°C confirmed the considerable elongation of 440%. This indicates that superplastic deformation occurred during dynamic recrystallization and decomposition of α phase colonies. Therefore, the mentioned phenomena are the main softening mechanisms that accelerate superplasticity in the alloy. The microstructure of the tip fracture region and grip region ($\varepsilon \cong 0.5$) of the specimen deformed at 850°C and the tip fracture region of the specimens deformed at 900 and 950°C are shown in Fig. 6. As seen in Fig. 6a, the microstructure of the grip section at 850°C consists of a 58.7% fine and globular α phase with an average grain size of 2.7 μm. Whereas, the tip fracture section at 850°C only consists of the equiaxed β grain with an average grain size of 43 μm. It can be deduced that the globular α phase was removed entirely in tip fracture at 850°C, while the β-transus temperature of the alloy was estimated as 930 ± 10°C. Therefore, the β-transus temperature of the alloy under the influence of superplastic deformation is shifted to lower temperatures in the range of 800–850°C. This could be attributed to deformation-induced transformation (DIT) in the alloy. Recently, the dynamic transformation behavior of Ti alloys was investigated by Jonas et al. [12]. They reported that the volume fraction of the β phase increased to 20% by deformation in the temperature range of 975–1025°C and a large strain of 1. Koike et al. [16] also observed that the β-transus temperature of Ti–5.5Al–1.5Fe alloy decreased to nearly 100°C due to the DIT at

727–927°C and a large strain of 2.2. Researchers [38–40] reported DIT during hot deformation of titanium alloys, as well. They believed that deformation at the temperature below the β-transus temperature of the alloys plays an essential role in $\alpha \rightarrow \beta$ transformation kinetics and morphology of phases. By increasing the deformation temperature in the single β phase region, only the equiaxed β grains could be observed in the microstructures. As seen in Fig. 6c, in the tip fracture of the specimen due to the removal of α, significant β grain growth leading to an increase in the average grain size to 75 μm at 950°C. In titanium alloys such as Ti–6Al–V, the volume fraction of the β phase at optimal superplastic temperature is four times higher than that at room temperature. Due to differences in the basic crystallography of α and β phases, the deformation behavior of each phase is substantially dissimilar. At elevated temperatures, the β phase is considerably softer than the α phase. As mentioned before, this effect is generally attributed to a higher diffusivity and more active slip systems in the β phase than in the α phase. Therefore, in either diffusion or dislocation accommodated superplasticity, it can be reasonable to assume that the volume fraction of the β phase plays an important role in determining the dominant mechanism of superplasticity [5].

Since the β phase in the α/β Ti alloys represents significantly lower flow stress than the α phase, deformation of the β phase is constrained by the α phase in the iso-strain mode. Consequently, the deformation characteristics of α/β titanium alloys are principally controlled by the α phase. However, in the iso-stress mode, the deformation is controlled by the deformation of the β phase [40]. The α phase has fewer slip systems and a self-diffusivity, approximately 100 orders slower than the β phase. Hence, it can be expected that the more significant volume fraction of the β phase causes a greater extent of superplasticity. However, the rate of grain growth in α/β Ti alloys containing a large volume fraction of the softer β phase is high, and a substantial volume fraction of the harder α phase is required to minimize the rate of grain growth. The optimal β phase volume fraction in α/β Ti alloys is 40% [41]. Studies [40] by TEM showed that in Ti–6Al–4V alloy, the accommodation mechanisms for grain/phase boundary sliding of the α and β phases are related to the dislocation motion. Lin et al. [3] using TEM, showed that the density of dislocations adjacent to the grain boundaries of Ti–6Al–4V and SP-700 alloys is high as the significant plastic strain caused by slip in the β grain. Thus, the accommodation mechanism for grain/phase boundary sliding in α and β phases of the SP-700 alloy can be related to dislocation motion. Figure 7 shows the grain boundary cracks formation at β/β boundaries in the specimen deformed at temperatures of 950°C. It can be suggested that the lower elongation at deformation region of 900–950°C is related to the formation of intergranular cracks due to the grain boundary single of

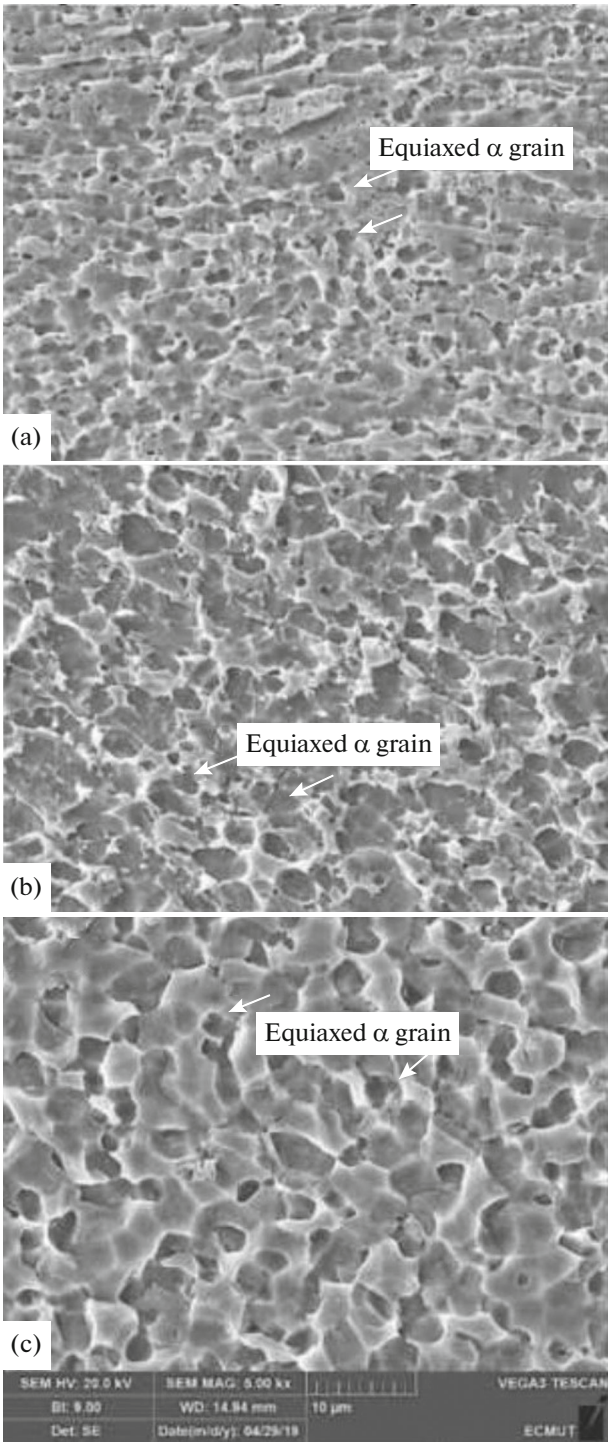

Fig. 5. The SEM image of the microstructure of the specimens deformed at strain rate of 0.005 s^{-1} and temperatures of: (a) 700, (b) 750, and (c) 800°C.

β phase. The microstructural characteristics of the specimens deformed at various temperatures and a strain rate of 0.005 s^{-1} are summarized in Table 1. The α phase volume fraction of the deformed specimens obtained nearly 62–69%. Hence, the β phase volume

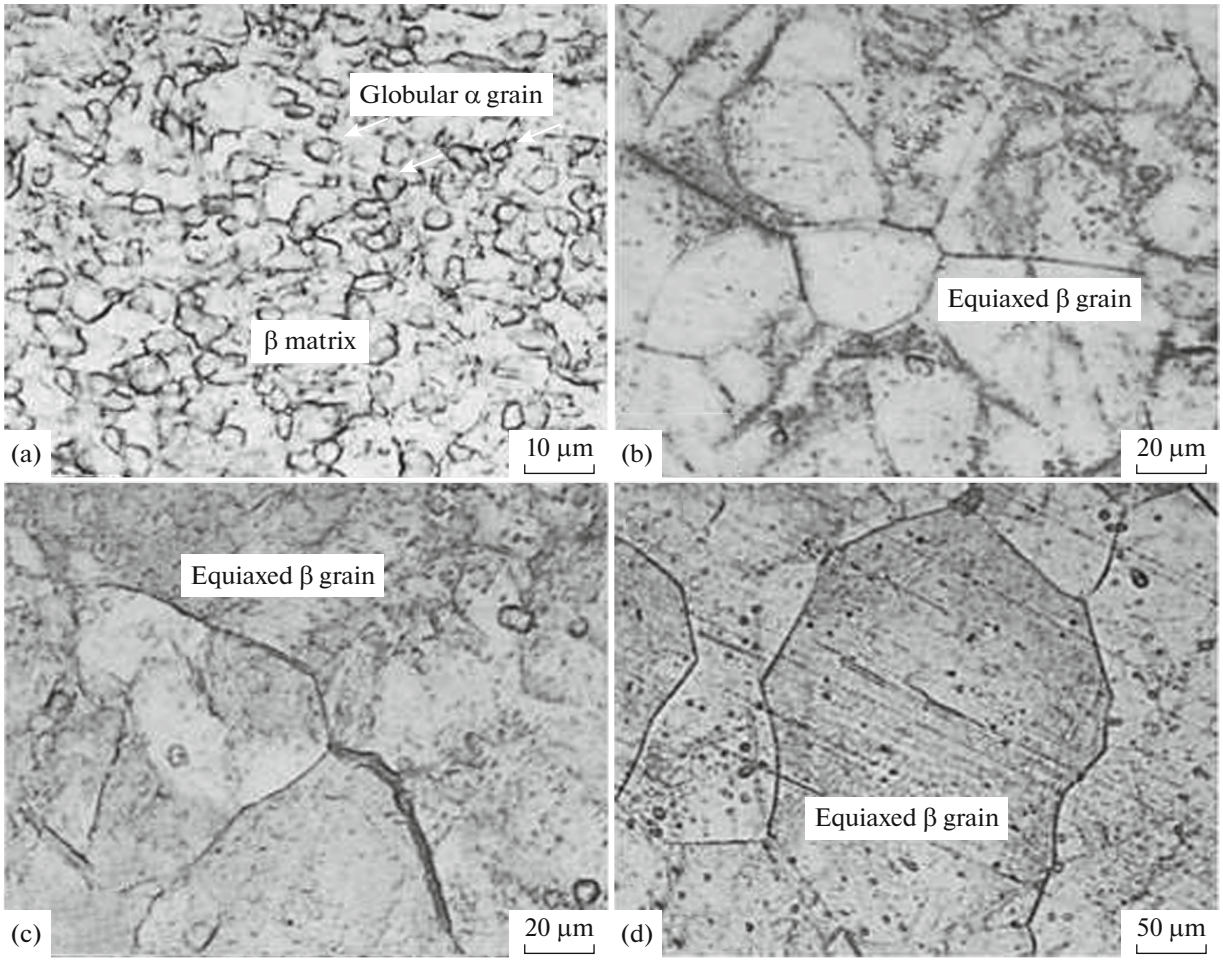

Fig. 6. The OM image of the microstructure of the specimen deformed at 850°C at the (a) tip fracture, (b) grip region, and the tip fracture region of the specimens deformed at (c) 900, and (d) 950°C.

fraction is 31–38% which is comparable to the optimum volume fraction of the β phase in α/β Ti alloys [41]. The relationship between the grain size in the tip fracture of the specimens and the deformation temperature can also be found in Table 1. The high elongations of 427–440% and favorable grain refinement were obtained at 750–800°C. The capability of the alloy in uniform tensile deformation decreased, and the lower elongations of 250–325% were obtained by removing the α phase in the β region due to significant β grain growth. Thus, the superplastic behavior of the alloy is in agreement with its microstructure.

Table 1. The microstructural characteristics of the deformed specimens

T, °C	Average grain size, μm	Phases	Morphology	Volume faction of α, %
700	2.3	α + β	Equiaxed α	69.2
750	2.4	α + β	Equiaxed α	67.5
800	6.8	α + β	Equiaxed α	61.5
850	43	β	Equiaxed β	–
900	52	β	Equiaxed β	–
950	75	β	Equiaxed β	–

4. SUPERPLASTICITY MECHANISM

The steady-state deformations of materials at high temperatures are defined as below [42]:

$$\dot{\varepsilon} = A\frac{DEb}{kT}\exp\left(-\frac{Q}{RT}\right)\left(\frac{b}{d}\right)^{p}\left(\frac{\sigma}{E}\right)^{n},$$

where D, E, b, T are diffusion coefficient, Young's modulus, the Burger's vector, and absolute temperature, respectively. Besides, d, σ, n, are grain size, the applied stress, and stress exponent, respectively; p is the characteristic of deformation mechanism, and Q is the activation energy for the rate-controlling process. A, R, k, are a constant, the the gas constant, and Boltzmann's constant. The n, p, and Q are critical parameters in determining the deformation mechanism. The mechanism depends on the calculated

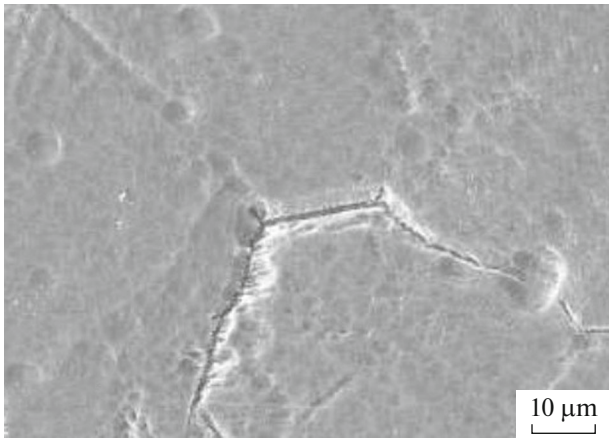

Fig. 7. The SEM image of the microstructure showed the inter-granular cracks in the specimen deformed at temperature of 950°C.

parameters, microstructural characters and comparison them with the physical models [43]. The superplastic parameters obtained from hot compression tests are summarized in Table 2.

The Q in the dual-phase α/β region is higher than that in the single-phase β region due to dynamic globularization of the lamellar α phase. The m values in the α/β and β regions were obtained as 0.36 to 0.38, and 0.33 to 0.34, respectively. Therefore, the n values in the α/β and β regions were measured as 2.6 to 2.8, and 2.9 to 3, respectively. However, the p value could not be obtained since the only one grain size was evaluated in the alloy. There are two important theories for GBS accommodation mechanisms [43, 44]: Rachinger mechanism supposed that sliding is accommodated by dislocations motion. However, Lifshitz mechanism assumed that sliding is a consequence of diffusion [45]. The Rachinger grain boundary sliding mechanism is more acceptable in the single phase β region due to the deformation parameters achieved as $m \approx 0.33$ (i.e. $n \approx 3$), $Q = Q_L$ (179–187 kJ/mol), and near-equiaxed grains of β phase. However, in the dual-phase α/β region DRX and decomposition of α colonies encourage the superplastic behavior of the alloy; Since the m value and Q becomes higher.

Table 2. Deformation parameters obtained from the hot compression tests of the SP-700 alloy

T, °C	m	$n = 1/m$	Q, kJ/mol
700	0.36	2.8	267
800	0.38	2.6	299
850	0.34	2.9	187
900	0.34	2.9	180
950	0.33	3	179

5. CONCLUSIONS

(1) At 750 and 800°C, typical superplastic deformation occurs. The maximum elongation of 440% is obtained at 800°C, where the strain rate sensitivity became 0.38. Hence, the m value distribution map of the SP-700 alloy could predict the optimal condition for the superplastic deformation.

(2) The highest m value was obtained in the temperature range of 770–820°C and strain rates of 0.001–0.01 s^{-1}.

(3) The microstructures of the alloy in the temperature range of 700–800°C consist of the globular α phase. However, it was removed entirely in the tip fracture of the specimen superplastically deformed at 900°C.

(4) In the single phase β region, the m value of 0.33, the similarity between the estimated Q and Q_L, and appearance of near-equiaxed β grains suggested that Rachinger GBS mechanism is the dominant phenomenon during deformation of the SP-700 alloy tested in this work.

(5) In the dual-phase α/β region, the higher m and Q values proposed that DRX and decomposition of α colonies encourage the superplasticity in the alloy.

FUNDING

This work was supported by ongoing institutional funding. No additional grants to carry out or direct this particular research were obtained.

CONFLICT OF INTEREST

The authors of this work declare that they have no conflicts of interest.

REFERENCES

1. M. J. Tan and S. F. Hassan, "High temperature deformation of Ti SP-700," in *Ti-2007 Science and Technology* (2007), pp. 567–570.
2. E. Alabort, P. Kontis, D. Barba, K. Dragnevski, and R. C. Reed, "On the mechanisms of superplasticity in Ti–6Al–4V," Acta Mater. **105**, 449–463 (2016). https://doi.org/10.1016/j.actamat.2015.12.003
3. M. L. Meier, D. R. Lesuer, and A. K. Mukherjee, "α Grain size and β volume fraction aspects of the superplasticity of Ti-6Al-4V," Mater. Sci. Eng., A **136**, 71–78 (1991). https://doi.org/10.1016/0921-5093(91)90442-p
4. J. Shen, Yu. Sun, Yo. Ning, H. Yu, Z. Yao, and L. Hu, "Superplasticity induced by the competitive DRX between BCC beta and HCP alpha in Ti–4Al–3V–2Mo–2Fe alloy," Mater. Charact. **153**, 304–317 (2019). https://doi.org/10.1016/j.matchar.2019.05.014
5. R. Boyer, G. Welsch, and E. W. Collings, *Materials Property Handbook: Ti Alloys* (ASM International, 1994).

6. Yi-H. Lin, Sh.-M. Wu, F.-H. Kao, Sh.-H. Wang, J.-R. Yang, Ch.-Ch. Yang, and Ch.-Sh. Chiou, "Microtwin formation in the α phase of duplex titanium alloys affected by strain rate," Mater. Sci. Eng., A **528**, 2271–2276 (2011). https://doi.org/10.1016/j.msea.2010.12.027
7. H. Fukai, A. Ogawa, K. Minakawa, H. Sato, and T. Tsuzuku, "Hot forming characteristics of SP-700 alloy," in *Ti-2003 Science and Technology* (2003), pp. 635–642.
8. E. Alabort, D. Barba, and R. Reed, "Mechanisms of superplasticity in titanium alloys: Measurement, in situ observations and rationalization," Defect Diffus. Forum **385**, 65–71 (2018). https://doi.org/10.4028/www.scientific.net/ddf.385.65
9. S. Biswas, B. Beausir, L. S. Toth, and S. Suwas, "Evolution of texture and microstructure during hot torsion of a magnesium alloy," Acta Mater. **61**, 5263–5277 (2013). https://doi.org/10.1016/j.actamat.2013.05.018
10. Y. Q. Ning, X. Luo, H. Q. Liang, H. Z. Guo, J. L. Zhang, and K. Tan, "Competition between dynamic recovery and recrystallization during hot deformation for TC18 titanium alloy," Mater. Sci. Eng., A **635**, 77–85 (2015). https://doi.org/10.1016/j.msea.2015.03.071
11. P. J. Bania, "Beta titanium alloys and their role in the titanium industry," JOM **46** (7), 16–19 (1994). https://doi.org/10.1007/bf03220742
12. J. J. Jonas, C. Aranas, A. Fall, and M. Jahazi, "Transformation softening in three titanium alloys," Mater. Des. **113**, 305–310 (2017). https://doi.org/10.1016/j.matdes.2016.10.039
13. R. D. K. Misra, J. Hu, I. V. S. Yashwanth, V. S. A. Challa, L.-X. Du, G.-S. Sun, and H. Xie, "Phase reverted transformation-induced nanograined microalloyed steel: Low temperature superplasticity and fracture," Mater. Sci. Eng., A **668**, 105–111 (2016). https://doi.org/10.1016/j.msea.2016.05.052
14. L. Huang, P. Hua, W. Sun, F. Liu, and F. Qi, "Necking characteristics and dynamic recrystallization during the superplasticity of IN718 superalloy," Mater. Sci. Eng., A **647**, 277–286 (2015). https://doi.org/10.1016/j.msea.2015.09.040
15. A. H. Sheikhali, M. Morakkabati, and S. M. Abbasi, "Constitutive modeling for hot working behavior of SP-700 titanium alloy," J. Mater. Eng. Perform. **28**, 6525–6537 (2019). https://doi.org/10.1007/s11665-019-04355-x
16. J. Koike, Y. Shimoyama, I. Ohnuma, T. Okamura, R. Kainuma, K. Ishida, and K. Maruyama, "Stress-induced phase transformation during superplastic deformation in two-phase Ti–Al–Fe alloy," Acta Mater. **48**, 2059–2069 (2000). https://doi.org/10.1016/s1359-6454(00)00049-5
17. G. E. Dieter, H. A. Kuhn, and S. L. Semiatin, *Handbook of Workability and Process Design* (ASM International, 2003).
18. A. Ogawa, M. Niikura, C. Ouchi, K. Minikawa, and M. Yamada, "Development and applications of titanium alloy SP-700 with high formability," J. Test. Eval. **24**, 100–109 (1996). https://doi.org/10.1520/JTE12683J
19. A. Wisbey, B. Geary, D. P. Davies, and C. M. Ward-Close, "Superplastic deformation and diffusion bonding of the low deformation temperature titanium alloy SP700," Mater. Sci. Forum **170–172**, 293–298 (1994). https://doi.org/10.4028/www.scientific.net/msf.170-172.293
20. B. Gershon and I. Eldror, "Superplastic sheet forming of aircraft parts from Ti-alloys," in *Ti-2007 Science and Technology* (2007), pp. 1287–1290.
21. A. H. Sheikhali, M. Morakkabati, and S. M. Abbasi, "Hot torsion behavior of SP-700 near beta titanium alloy in single and dual phase regions," Int. J. Mater. Res. **109**, 1136–1145 (2018). https://doi.org/10.3139/146.111715
22. A. H. Sheikhali and M. Morakabati, "Hot working of SP-700 with lamellar structure using a processing map," Int. J. Mater. Res. **111**, 297–306 (2020).
23. *AMS 4964C, Ti Alloy Bars, Wire, Forgings, and Rings Ti–4.5Al–3V–2Fe–2Mo Annealed* (2011).
24. Z. Guo, S. Malinov, and W. Sha, "Modelling beta transus temperature of titanium alloys using artificial neural network," Comput. Mater. Sci. **32**, 1–12 (2005). https://doi.org/10.1016/j.commatsci.2004.05.004
25. P. M. Souza, H. Beladi, R. Singh, B. Rolfe, and P. D. Hodgson, "Constitutive analysis of hot deformation behavior of a Ti6Al4V alloy using physical based model," Mater. Sci. Eng., A **648**, 265–273 (2015). https://doi.org/10.1016/j.msea.2015.09.055
26. *ASTM E209-00, Standard Practice for Compression Tests of Metallic Materials at Elevated Temperatures with Conventional or Rapid Heating Rates and Strain Rates* (ASTM International, 2010).
27. *ASTM E3-11, Standard Guide for Specimens* (ASTM International, West Conshohocken, Pa., 2011).
28. I. Balasundar, T. Raghu, and B. P. Kashyap, "Modeling the hot working behavior of near-α titanium alloy IMI 834," Prog. Nat. Sci.: Mater. Int. **23**, 598–607 (2013). https://doi.org/10.1016/j.pnsc.2013.11.004
29. K. A. Padmanabhan, R. A. Vasin, and F. U. Enikeev, *Superplastic Flow: Phenomenology and Mechanics*, Engineering Materials (Springer, Berlin, 2001). https://doi.org/10.1007/978-3-662-04367-7
30. H. Q. Liang, Y. Nan, Y. Q. Ning, H. Li, J. L. Zhang, Z. F. Shi, and H. Z. Guo, "Correlation between strain-rate sensitivity and dynamic softening behavior during hot processing," J. Alloys Compd. **632**, 478–485 (2015). https://doi.org/10.1016/j.jallcom.2014.12.270
31. O. Sivakesavam and Y. V. R. K. Prasad, "Characteristics of superplasticity domain in the processing map for hot working of as-cast Mg–11.5Li–1.5Al alloy," Mater. Sci. Eng., A **323**, 270–277 (2002). https://doi.org/10.1016/s0921-5093(01)01392-2
32. V. G. Krishna, Y. V. R. K. Prasad, N. C. Birla, and G. Rao, "Processing map for the hot working of near-α titanium alloy 685," J. Mater. Process. Technol. **71**, 377–383 (1997). https://doi.org/10.1016/s0924-0136(97)00102-7
33. P. Wanjara, M. Jahazi, H. Monajati, S. Yue, and J.-P. Immarigeon, "Hot working behavior of near-α al-

loy IMI834," Mater. Sci. Eng., A **396**, 50–60 (2005). https://doi.org/10.1016/j.msea.2004.12.005

34. I. Philippart and H. J. Rack, "High temperature dynamic yielding in metastable Ti–6.8Mo–4.5F–1.5Al," Mater. Sci. Eng., A **243**, 196–200 (1998). https://doi.org/10.1016/s0921-5093(97)00800-9
35. A. H. Sheikhali, M. Morakkabati, S. M. Abbasi, and A. Rezaei, "Superplasticity of coarse-grained Ti–13V–11Cr–3Al alloy," Int. J. Mater. Res. **104**, 1122–1127 (2013). https://doi.org/10.3139/146.110965
36. Q. J. Sun, G. C. Wang, and M. Q. Li, "The superplasticity and microstructure evolution of TC11 titanium alloy," Mater. Des. **32**, 3893–3899 (2011). https://doi.org/10.1016/j.matdes.2011.02.062
37. J. S. Kim, J. H. Kim, Y. T. Lee, C. G. Park, and C. S. Lee, "Microstructural analysis on boundary sliding and its accommodation mode during superplastic deformation of Ti–6Al–4V alloy," Mater. Sci. Eng., A **263**, 272–280 (1999). https://doi.org/10.1016/s0921-5093(98)01157-5
38. H. Z. Niu, F. T. Kong, Y. Y. Chen, and C. J. Zhang, "Low-temperature superplasticity of forged Ti–43Al–4Nb–2Mo–0.5B alloy," J. Alloys Compd. **543**, 19–25 (2012). https://doi.org/10.1016/j.jallcom.2012.07.127
39. L. He, A. Dehghan-Manshadi, and R. J. Dippenaar, "The evolution of microstructure of Ti–6Al–4V alloy during concurrent hot deformation and phase transformation," Mater. Sci. Eng., A **549**, 163–167 (2012). https://doi.org/10.1016/j.msea.2012.04.025
40. A. Dehghan-Manshadi and R. J. Dippenaar, "Strain-induced phase transformation during thermo-mechanical processing of titanium alloys," Mater. Sci. Eng., A **552**, 451–456 (2012). https://doi.org/10.1016/j.msea.2012.05.069
41. J. Pilling and N. Ridley, *Superplasticity in Crystalline Solids* (The Inst. of Met. Publ., London, 1989).
42. A. K. Mukherjee, J. E. Bird, and J. E. Dorn, "Experimental correlations for high-temperature creep," Trans. Am. Soc. Met. **62**, 155–164 (1969).
43. Z. Ma and R. S. Mishra, "Superplastic deformation mechanism," in *Friction Stir Superplasticity for Unitized Structures* (Butterworth-Heinemann, New York, 2014), pp. 39–57. https://doi.org/10.1016/B978-0-12-420006-7.00006-6
44. W. A. Rachinger, "Relative grain translations in the plastic flow of Al," J. Inst. Met. **81** (1952).
45. I. M. Lifshitz, "On the theory of diffusion-viscous flow of polycrystalline bodies," Sov. Phys. **17**, 909–920 (1963).